

# Frequency and potential dependence of reversible electrocatalytic hydrogen interconversion by [FeFe]-hydrogenases

Kavita Pandey<sup>a,b</sup>, Shams T. A. Islam<sup>a</sup>, Thomas Happe<sup>c</sup>, and Fraser A. Armstrong<sup>a,1</sup>

<sup>a</sup>Inorganic Chemistry Laboratory, Department of Chemistry, University of Oxford, Oxford OX1 3QR, United Kingdom; <sup>b</sup>School of Solar Energy, Pandit Deendayal Petroleum University, Gandhinagar 382007, Gujarat, India; and <sup>c</sup>AG Photobiotechnology Ruhr-Universität Bochum, 44801 Bochum, Germany

Edited by Thomas E. Mallouk, The Pennsylvania State University, University Park, PA, and approved March 2, 2017 (received for review December 5, 2016)

The kinetics of hydrogen oxidation and evolution by [FeFe]-hydrogenases have been investigated by electrochemical impedance spectroscopy—resolving factors that determine the exceptional activity of these enzymes, and introducing an unusual and powerful way of analyzing their catalytic electron transport properties. Attached to an electrode, hydrogenases display reversible electrocatalytic behavior close to the  $2\text{H}^+/\text{H}_2$  potential, making them paradigms for efficiency: the electrocatalytic “exchange” rate (measured around zero driving force) is therefore an unusual parameter with theoretical and practical significance. Experiments were carried out on two [FeFe]-hydrogenases, CrHydA1 from the green alga *Chlamydomonas reinhardtii*, which contains only the active-site “H cluster,” and Cpl from the fermentative anaerobe *Clostridium pasteurianum*, which contains four low-potential FeS clusters that serve as an electron relay in addition to the H cluster. Data analysis yields catalytic exchange rates (at the formal  $2\text{H}^+/\text{H}_2$  potential, at 0 °C) of 157 electrons (78 molecules  $\text{H}_2$ ) per second for Cpl and 25 electrons (12 molecules  $\text{H}_2$ ) per second for CrHydA1. The experiments show how the potential dependence of catalytic electron flow comprises frequency-dependent and frequency-independent terms that reflect the proficiencies of the catalytic site and the electron transfer pathway in each enzyme. The results highlight the “wire-like” behavior of the Fe-S electron relay in Cpl and a low reorganization energy for electron transfer on/off the H cluster.

hydrogen | electrocatalysis | impedance spectroscopy | hydrogenase | electron transfer

Despite their giant size, many redox enzymes are now established as reversible electrocatalysts through investigations by protein film electrochemistry (PFE) (1). Attached to an electrode, these enzymes catalyze rapid oxidation and reduction, with only a minimum overpotential being required to swap the current direction either side of the equilibrium potential (2–5). Of particular interest are hydrogenases, which catalyze the oxidation and production of  $\text{H}_2$  with activities that may rival platinum (6–11) and are inspirational in the quest for future electrocatalysts as well as in artificial photosynthesis (12, 13).

The enzymes known as [FeFe]-hydrogenases contain a unique bimetallic active site known as the H cluster (Fig. 1), which contains six Fe atoms in two domains: a 2Fe domain that is the site for  $\text{H}_2$  activation and a [4Fe–4S] cluster domain that presumably acts as the immediate electron donor/acceptor and internal electron buffer within the H cluster (14–16). Key representatives are hydrogenase 1 from a fermentative anaerobe *Clostridium pasteurianum* (Cpl) and hydrogenase A1 from a photosynthetic alga *Chlamydomonas reinhardtii* (CrHydA1). Fig. 1 shows that Cpl contains an electron transfer relay consisting of three [4Fe–4S] clusters and one [2Fe–2S] cluster (17). The assumed natural redox partner of Cpl is a 2[4Fe–4S] ferredoxin (18). The internal relay allows long-range electron transport (ET) between the H cluster and the protein surface, and it may be significant that it branches into two pathways that could provide improved coupling to an electrode surface. In contrast,

CrHydA1 contains only the H cluster: in the living cell, it receives electrons from photosystem I via a small [2Fe–2S] ferredoxin known as PetF (19). No accessory internal Fe–S clusters are present to mediate or store electrons.

For enzymes, PFE has focused entirely on net catalytic electron flow that is observed as direct current (DC) in voltammograms (2, 3, 10). Use of DC cyclic voltammetry as opposed to single potential sweeps alone helps to distinguish rapid, steady-state catalytic activity at different potentials from relatively slow, potential-dependent changes in activity that are revealed as hysteresis (10). However, only net electron flow is observed and little information is obtained on certain inherent factors that underline the reversible nature of the catalysis. For example, it would be significant to know how rapidly the catalytic cycle can turn back and forth at the equilibrium potential: this unusual quantity is related to the familiar exchange current for an electrode reaction that is obtained by extrapolating the exponential current–overpotential relationship (a Tafel plot) and is the catalytic remnant of the Marcus electron self-exchange rate (at zero driving force) (20). In reality, the electrocatalytic exchange constant encompasses a combination of long-range electron transfer efficiency and inherent catalytic proficiency of the active site, and cannot be extracted directly by voltammetric methods. Additionally, to understand the “design principles” of an electron transport enzyme, it is highly relevant to measure and resolve the responses to a bias, analogous to electronic circuitry: we might thus distinguish between limitations due to time-dependent chemical steps occurring at the active site from those due to the properties of relay sites that mediate long-range ET in what is

## Significance

Hydrogenases are among the most active of enzymes, with active sites that compare with platinum metals in regard to rates of hydrogen production and oxidation. Attached to an electrode, [FeFe]-hydrogenases behave as reversible electrocatalysts close to the equilibrium potential, with only a minimal overpotential being required to oxidize  $\text{H}_2$  or reduce protons. Electrochemical impedance spectroscopy, which uses a small amplitude potential modulation over a wide frequency range, has been used to measure the “electrocatalytic exchange rate”—the “idle speed” at which the cycle runs back and forth at the formal potential. The results also quantify the efficacy of Fe–S clusters, at the active site or in the relay, in controlling the rates of catalytic electron flow.

Author contributions: K.P. and F.A.A. designed research; K.P. and S.T.A.I. performed research; T.H. contributed new reagents/analytic tools; K.P., S.T.A.I., and F.A.A. analyzed data; and K.P., S.T.A.I., T.H., and F.A.A. wrote the paper.

The authors declare no conflict of interest.

This article is a PNAS Direct Submission.

<sup>1</sup>To whom correspondence should be addressed. Email: fraser.armstrong@chem.ox.ac.uk.

This article contains supporting information online at [www.pnas.org/lookup/suppl/doi:10.1073/pnas.1619961114/-DCSupplemental](http://www.pnas.org/lookup/suppl/doi:10.1073/pnas.1619961114/-DCSupplemental).

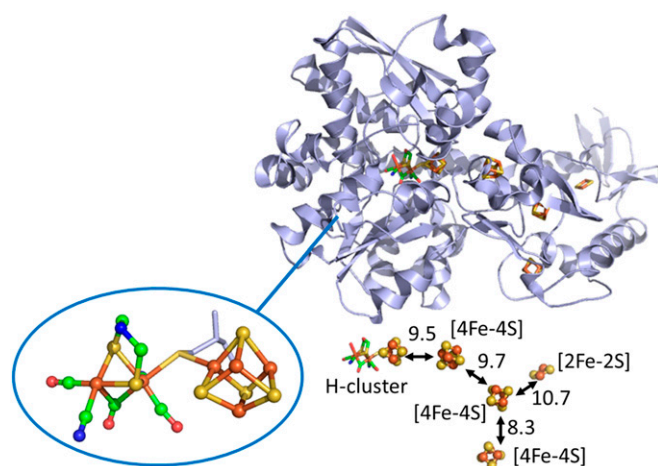


**Fig. 1.** Structure of the [FeFe]-hydrogenase I (Cpl) from *Clostridium pasteurianum*, Protein Data Bank (PDB) ID code 3C8Y. A close-up view of the active site H cluster is also shown (Lower Left) along with the [FeS]-cluster relay and intersite distances (Lower Right) measured in angstrom units.

often casually referred to as “wire-like” conductivity. Such information can be obtained by electrochemical impedance spectroscopy (EIS), which uses a small-amplitude sinusoidal AC voltage to measure the impedance components at given values of the electrode potential (20–23). Impedance is generalized resistance and the opposite of conductance—the electronic term expressing the ease of electron flow. We have now used EIS to study CrHydA1 and Cpl: our goals have been to determine, quantitatively, the catalytic proficiency of the H cluster in terms of electrocatalytic exchange rate, and to examine the influence of the electron relay in mediating long-range electron transfer.

## Results and Discussion

**Cyclic Voltammetry.** All experiments were carried out at 0 °C, with 0.10 M sodium phosphate buffer at pH 7.0, under strictly anaerobic conditions, using a rotating disk pyrolytic graphite edge (PGE) electrode at which Cpl and CrHydA1 adsorb tightly on the rough surface in a highly electroactive state (2). Under 100% H<sub>2</sub>, catalytic activity is close to optimal for each enzyme and electrode rotation at 1,000 rpm ensured that H<sub>2</sub> mass transport is not limiting (24). The catalytic electrochemistry of Cpl and CrHydA1 is highly reproducible (Fig. 2) (24). In either case, the steady-state catalytic current (red traces) changes direction sharply either side of the equilibrium 2H<sup>+</sup>/H<sub>2</sub> potential, justifying the description of [FeFe]-hydrogenases as reversible electrocatalysts with Pt-like activity. There are notable differences: Cpl appears particularly efficient at catalyzing H<sub>2</sub> evolution, whereas the H<sub>2</sub> oxidation current levels off within 0.2 V of the reversible value. Although not cutting the *x* axis as sharply as Cpl, CrHydA1 catalyzes both H<sub>2</sub> production and H<sub>2</sub> oxidation reactions at similar rates for a given overpotential. At more positive potentials, both hydrogenases undergo conversion to an inactive oxidized form, the conversion being more rapid for CrHydA1 and evident from the hysteresis observed during H<sub>2</sub> oxidation; hence, we restricted EIS measurements to an upper potential limit of 0 V vs. SHE. Both hydrogenases are inhibited by carbon monoxide, which binds tightly at a potential more positive than −0.5 V but is released at a potential below −0.6 V (24, 25). This inhibition provides a benign and reversible “on/off switch” by which to identify the impedance components that are unique to electrocatalysis.

## Electrochemical Impedance Spectroscopy.

**Nyquist spectra at equilibrium potential.** Detailed insight into the processes taking place at the enzyme-modified electrodes was

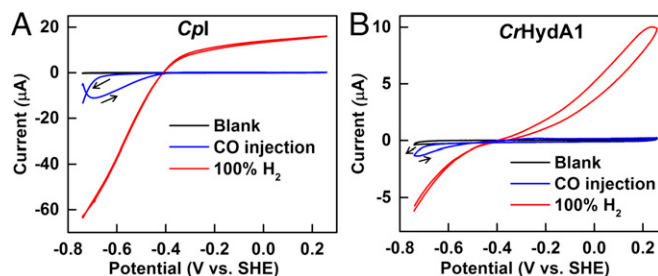


**Fig. 2.** Cyclic voltammetry profiles of [FeFe]-hydrogenases, Cpl (A) and CrHydA1 (B), on PGE electrodes and equilibrated with 100% H<sub>2</sub> flowing in the headspace (red trace): the trace shows that, depending upon the potential applied, both H<sub>2</sub> oxidation and H<sup>+</sup> reduction are carried out by the enzyme. When CO is injected, the enzymes are unable to carry out H<sub>2</sub> oxidation, and H<sup>+</sup> reduction begins at a more negative potential (below −0.6 V vs. SHE) where CO is released (blue trace). Conditions: pH 7.0 (0.10 M phosphate buffer); temperature, 0 °C; scan rate, 20 mV·s<sup>−1</sup>.

provided by EIS, where the system responds to the application of a small perturbation [10 mV root-mean-square (rms)] modulation over a range of frequencies at different potentials under steady-state conditions. The modulation amplitude was chosen as the best compromise to obtain conditions closest to the equilibrium potential without adverse noise. Fig. 3A shows EIS spectra for Cpl and CrHydA1 adsorbed at a PGE electrode under 1-bar H<sub>2</sub>, recorded at the equilibrium cell potential [the potential of zero net current, which we also define as the formal potential of the reversible hydrogen electrode (RHE)] in the frequency range of 0.1 Hz to 100 kHz. At high frequency (see expanded plot in Fig. 3B), the results obtained for Cpl and CrHydA1 are similar and resemble the results obtained for a blank PGE electrode and that observed when CO is introduced to inhibit electrocatalysis (shown for Cpl). The Nyquist spectra for both Cpl and CrHydA1 with CO inhibition almost overlay each other, and hence only data for Cpl are shown. The EIS spectra show similar high-frequency arcs (Fig. 3B) that deviate in behavior at lower frequencies to give almost straight lines in the case of blank and CO-inhibited enzymes, and semicircular arcs of different radii for the two enzymes catalyzing 2H<sup>+</sup>/H<sub>2</sub> interconversion.

**Modeling catalytic electron transport by equivalent circuit analysis.** The results and discussion are based upon the scheme shown in Fig. 4, which represents the entire catalytic charge transport process at the electrode–enzyme solution region in terms of an equivalent circuit diagram. The circuit consists of three components in series; the cell resistance, the impedance due to the electrical double layer, and the impedance that describes catalytic electron flow through the enzyme, each of which is revealed in turn as the

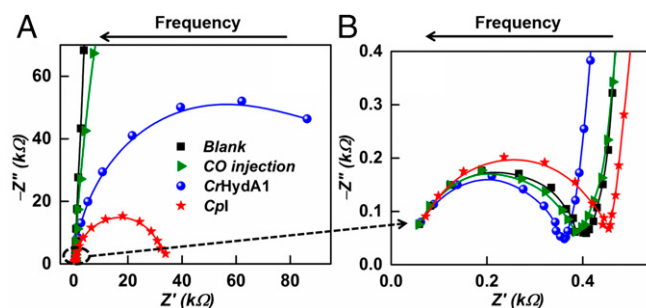


**Fig. 3.** (A) Impedance spectra of the [FeFe]-hydrogenase systems at the equilibrium potential. (B) Enlargement focusing on the high-frequency details. Conditions: pH 7.0 (0.10 M phosphate buffer); temperature, 0 °C. The symbols are experimental data points, and the lines represent the fits obtained.

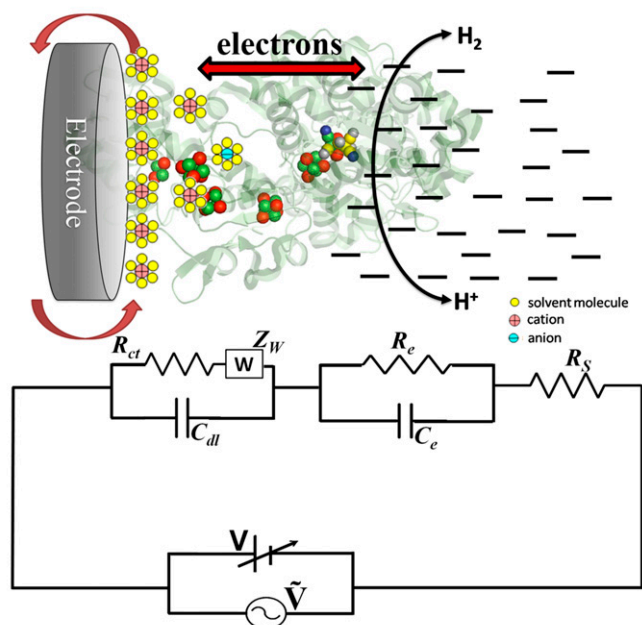


**Fig. 4.** Equivalent circuit used to fit the Nyquist spectra obtained for hydrogenases attached to an electrode, with a schematic showing the dominance of circuit elements in the different regions of charge transfer.

frequency is lowered. By considering all of the circuit elements, the net impedance at any point on the spectra is given as follows:  $Z = Z' + jZ''$ , where  $Z'$  and  $Z''$  are the real and imaginary components of EIS (26, 27). Algebraic manipulation of  $Z' + jZ''$  leads to values for resistance  $R$  and capacitance  $C$  at each given frequency. Further details are given in ESI.

**The cell resistance.** The cell resistance  $R_s$  was revealed from the extrapolated intercept of the high-frequency semicircle with the  $Z'$  axis and was the same for all experiments, which were conducted under the same conditions with the same electrochemical cell. The value is 57.5  $\Omega$ .

**The electrical double layer.** The high-frequency arc and mid-frequency portions of the EIS spectra are modeled by the cell elements  $R_{ct}$ ,  $C_{dl}$ , and  $W$ . The  $R_{ct}$  and  $C_{dl}$  elements describe the ion transport inside the double layer formed at the electrode, whereas  $W$  corresponds to the semiinfinite diffusion of the charged particles and has the form  $Z_W = \alpha / (j\omega)^{1/2}$  (22, 27). The arc intercepts the  $Z'$  axis at  $R_{ct} + R_s$ , and it is likely that the slightly differing values of  $R_{ct}$  reflect differences in the surface characteristics of the two enzymes. The fact that  $R_{ct}$  values vary so little provides confidence to interpret the remaining data, which relate to the specific electrocatalytic activities of each enzyme.

**Catalytic electron transport through the enzyme.** The low-frequency arc that appears when catalytic activity is not inhibited by CO shows that each enzyme molecule attached to the electrode behaves as a resistor and capacitor connected in parallel (20). To understand how this relates to electron flow back and forth through an enzyme attached to the electrode, we consider what is happening at the limits of the arc. At the high-frequency limit, the impedance response is simply  $R_{ct}$  and is similar for both enzymes with and without CO: even with uninhibited enzyme, the frequency is sufficiently high that the enzyme is unable to contribute through catalytic turnover. The response in the low-frequency region represents the resistance  $R_e$  to electron flow. The responses at intermediate frequencies across the arc reflect the increasing and decreasing contributions from the frequency-dependent catalytic activity as electrons are now able to flow back and forth between the electrode and  $H_2$  or  $H^+_{aq}$  in solution.

The frequency-independent resistance  $R_e$  quantifies the difficulty of moving electrons from the electrode to the active site and reflects such factors as distance, medium, and the influence of an FeS relay (28, 29). The frequency-dependent resistance arises from the capacitance  $C_e$  (as  $1/\omega C$ ): it reflects engagement of the cyclic contribution from reversible chemical steps ranging from binding/release of  $H_2$  to atom/ion transfer, as well as electron transfers that are tightly coupled to these steps (30, 31). Expressed another way,  $R_e$  represents the DC resistance always offered by the combined electron relay and active site, whereas  $C_e$  is analogous to a time-dependent charging and discharging of the active site (this is a Faradaic process because catalytic cycling allows electrons to flow). The variation of  $R_e$  and  $C_e$  with potential allows more in-depth interpretation of the electrocatalytic activity than is possible from voltammograms.

Quantitative values from EIS spectra at the equilibrium potential ( $E = 0$  V vs. RHE) were extracted by fitting the experimental data (23) and are summarized in Table 1. Agreement between the theoretical fits and the experimental Nyquist spectra is within 1.3%, and  $R_s$  has been independently fitted for each set of data. Most notably, the much lower  $R_e$  value for *CpI* compared with that for *CrHydA1* shows that electron flow through *CpI* is particularly facile. This result is as expected because *CpI* has an extensive relay system of low-potential FeS clusters to connect the H cluster with the distal [4Fe–4S] and [2Fe–2S] clusters that each lie within 8 Å of the accessible protein surface, whereas the H cluster of *CrHydA1* has no internal relay. In biology, the buried H cluster in *CrHydA1* must exchange electrons directly with a small protein—a ferredoxin known as PetF—in encounters that are necessarily transient but likely to be more efficient in regard to electronic coupling than achieved with an electrode. A calculated protein–protein structure suggests a distance of 11 Å between the H cluster of *CrHydA1* and the [2Fe–2S] cluster of PetF (32). Negligible differences between the blank and CO-inhibited enzymes, in the values of all of the elements, reflect the fact that the inhibitor CO acts as an excellent “off” switch in both cases (24): notably, noncatalytic electron transfers to and within the enzyme barely register in the EIS experiments.

**Determination of exchange current density.** The exchange current density  $i_0$  at the equilibrium cell potential was determined from the expression,  $i_0 = RT/nFR_e$ , where  $R$ ,  $T$ ,  $n$ , and  $F$  are the universal gas constant, temperature in Kelvin, overall number (=2) of electrons taking part in the reaction, and Faraday’s constant, respectively (33). In a typical experiment as just described, an exchange current density of 27.7  $\mu A \cdot cm^{-2}$  was obtained for *CpI*, whereas that of *CrHydA1* was nearly fivefold lower at 6.07  $\mu A \cdot cm^{-2}$ . To draw molecular-level conclusions from these data requires knowing the electroactive coverage  $\Gamma$  for each case (current density =  $n k_{ex} F \Gamma$ ) as this allows the exchange turnover frequency  $k_{ex}$  to be determined. However, neither *CpI* nor *CrHydA1* are present at high enough coverage to exhibit non-turnover signals that are due to simple, noncatalytic oxidation and reduction of internal electron transfer components. However, an independent value of  $k_{ex}$  could be determined from a Bode plot, an alternate means of presenting the data in which phase angle is plotted against frequency.

**Table 1.** Parameters obtained by fitting the experimental Nyquist spectra for the enzymes on PGE electrode (at equilibrium potentials) to yield equivalent circuits by MATLAB software

Condition	$R_s$ , $\Omega$	$R_{ct}$ , $\Omega$	$C_{dl}$ , $\mu F$	$R_e$ , $k\Omega$	$C_e$ , $\mu F$
Blank	57.5	350.2	0.031	—	—
CO inhibition	57.5	350.1	0.031	—	—
<i>CpI</i> ( $H_2$ )	57.5	410.7	0.022	28.6	14.8
<i>CrHydA1</i> ( $H_2$ )	57.5	338.3	0.038	119.8	10.8



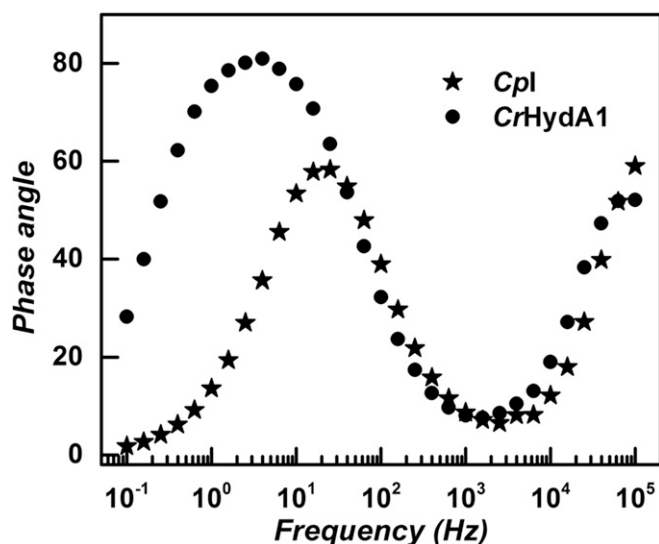


**Fig. 5.** Bode representations for the [FeFe]-hydrogenases poised at the equilibrium potential. Conditions: pH 7.0 (0.10 M phosphate buffer); temperature, 0 °C. The symbols are experimental data points, and the lines are included to guide the eye.

**Determination of catalytic exchange frequency: Analysis of Bode plots at the equilibrium potential.** Fig. 5 shows Bode plots for CpI and CrHydA1 at the equilibrium potential. The time constant at the peak maxima is related to the electrocatalytic exchange rate constant  $k_{ex}$ . For CpI, the peak in the phase angle corresponds to a higher frequency ( $f$ ) than for CrHydA1, signifying a smaller time

constant. Quantitatively, using  $k_{ex} = 2\pi f$ , the  $k_{ex}$  values for CpI and CrHydA1 are 157 and 25  $s^{-1}$ , corresponding to 78 and 12 molecules  $H_2$  per second, respectively. These are useful but approximate values erring on the high side, as the modulation amplitude (10 mV rms equates to  $E_{eq} \pm 5$  mV) can never be zero.

By backcalculation, the  $k_{ex}$  values allow estimation of the electroactive coverage in the experiment conducted. We obtained  $0.91 \times 10^{-12}$  mol·cm $^{-2}$  for CpI, and  $1.26 \times 10^{-12}$  mol·cm $^{-2}$  for CrHydA1. The low values are consistent with the inability to observe any signals due to Fe-S clusters under noncatalytic (CO-inhibited) conditions.

**Analysis of Nyquist spectra to resolve the dependences of catalytic turnover rate on potential.** Impedance measurements (Fig. 6) were carried out at various potentials from  $-1.0$  to  $-0.250$  V vs. saturated calomel electrode (SCE), the blue symbols corresponding to the equilibrium potential. Figs. S1 and S2 show how impedance spectroscopy measurements relate to the cyclic voltammograms at different potentials. For both CpI and CrHydA1, applying an increasing overpotential in the proton-reducing direction causes the low-frequency semicircles to contract in size and cut the x axis at increasingly lower  $Z'$  values on the right. However, CpI and CrHydA1 show completely different behavior upon increasing the overpotential in the  $H_2$  oxidation direction: whereas CrHydA1 displays the expected semicircle contraction, CpI shows a strong expansion.

Fig. 7A shows how  $R_e$  values vary within a narrow potential range ( $\pm 0.4$  V) on either side of the equilibrium value. The results were obtained by fitting the Nyquist spectra to the standard model for the circuit shown in Fig. 4. The two enzymes are distinguished by their contrasting behavior either side of the equilibrium potential (0 V vs. RHE): notably, the potential dependences of  $R_e$  closely mirror the DC voltammograms shown in

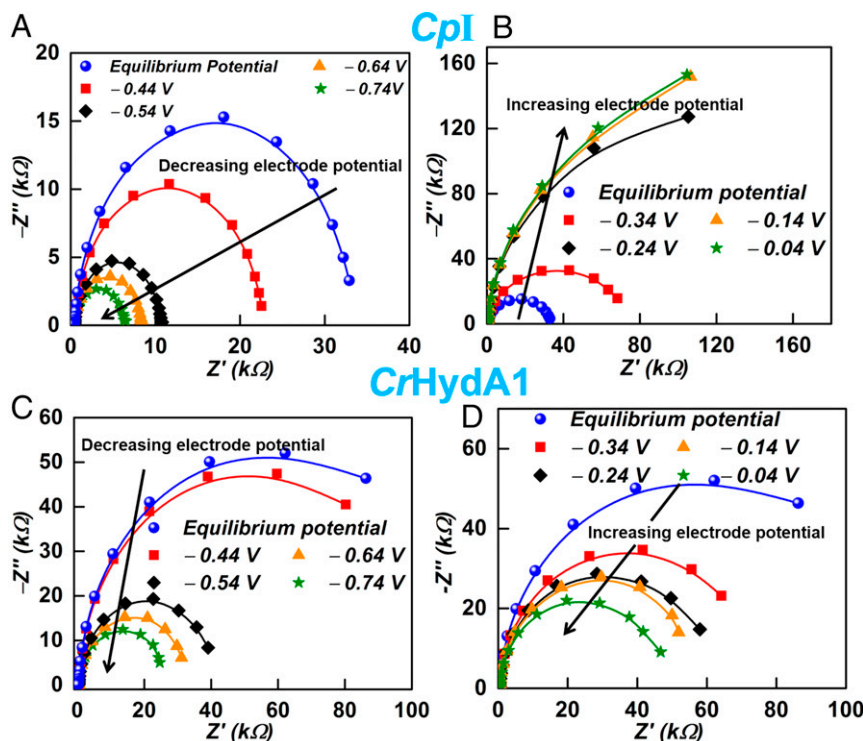


**Fig. 6.** Impedance measurements at various potentials vs. SHE: (A) at electrode potentials where CpI catalyzes net  $H^+$  reduction [black arrow signifies decreasing (more negative) electrode potential]; (B) at electrode potentials where CpI catalyzes the net oxidation of  $H_2$  [black arrow signifies increasing (more positive) electrode potential]; (C) at electrode potentials where CrHydA1 catalyzes net  $H^+$  reduction [black arrow signifies decreasing (more negative) electrode potential]; (D) at electrode potentials where CrHydA1 catalyzes the net oxidation of  $H_2$  [black arrow signifies increasing (more positive) electrode potential]. Conditions: pH 7.0 (0.10 M phosphate buffer), temperature, 0 °C. The symbols are experimental data points, and the lines are the theoretical fit.



with reorganization energy  $\lambda = 0.35$  eV gave a better fit (35), and a further improvement was obtained by introducing some dispersion (optimized at  $\beta d_0 = 11$ ; Fig. S3) that is expected in view of the complexity of protein interactions with the rough electrode surface (36). Although the MHC approach is approximate, and  $\lambda$  is likely to vary across the wide potential range where different intermediate states dominate, there is no doubt that it is more applicable than the BV model. A simulation and list of variables giving the best fit for *CpI* are given in Fig. S4 and Table S1. The electrocatalytic exchange rate for *CrHydA1* is thus controlled by long-range ET and the value of 12 molecules  $H_2$  per second must understate the inherent activity of the H cluster. Even at 0 °C, *CpI* attains a turnover frequency exceeding  $5,000\text{ s}^{-1}$  for  $H_2$  evolution (molecules  $H_2$  produced per molecule of enzyme) at  $\eta = 0.2$  V, whereas  $H_2$  oxidation is limited to below  $2,000\text{ s}^{-1}$ . The values may be compared with the broad result of  $21,000 \pm 12,000\text{ s}^{-1}$  for  $H^+$  reduction at 25 °C, pH 7.0 with  $\eta \sim 0.1$  V, reported for a similar enzyme (*HydA* from *Clostridium acetobutylicum*) (11). It is probable that similar rates would be observed for *CrHydA1* were long-range electron transfer to be more efficient, no doubt a result of the PGE electrode being a poor substitute for the natural ET partner *PetF* (19). As long realized, the H cluster is a superb catalyst of  $H_2$  activation; the low value for  $\lambda$  suggests that it is also optimized for electron transfer.

## Materials and Methods

*CpI* and *CrHydA1* were prepared as described previously, using the semi-synthetic procedure (37). All electrochemical experiments were carried out

using a Ivium CompactStat E800 workstation equipped with a frequency response analyzer. A PGE electrode was used as working electrode in the main thermostated (0 °C) compartment of a three-electrode cell, in which a Pt wire was used as the counterelectrode and a SCE contained in a Luggin capillary side arm maintained at room temperature was used as a nonisothermal reference (24). To form each film of enzyme, 1  $\mu\text{L}$  of 50  $\mu\text{M}$  enzyme solution was pipetted onto the freshly polished PGE electrode, and excess solution was removed after 1 min. The electrochemical cell was housed in a glove box (Vacuum Atmospheres,  $O_2 < 5$  ppm). The main compartment contained 0.10 M phosphate buffer at pH 7.0, and  $H_2$  gas (100%) was flowed through the cell headspace. The electrode was rotated at 1,000 rpm. Potentials were converted to the standard hydrogen scale using  $E_{\text{SHE}} = E_{\text{SCE}} + 241$  mV to relate to most literature available (20). A formal RHE scale was generated using the potential of zero net current. To switch off hydrogenase electrocatalysis, the flow of  $H_2$  was stopped, 5 mL of  $CO$ -saturated buffer was injected into the cell to give an initial concentration of 77  $\mu\text{M}$   $CO$ , and a potential of  $-250$  mV (vs. SCE) was applied for 5 min before recording impedance measurements (24). Due care was taken, for example, by conducting experiments at 0 °C, to maximize enzyme film stability, which was checked by recording a cyclic voltammogram after each set of impedance measurements.

**ACKNOWLEDGMENTS.** This research was supported by the ERASynBio Consortium "Sun2Chem." F.A.A. thanks the UK Biotechnology and Biological Sciences Research Council for funding (Grant BB/M005720/1). K.P. thanks the British Council for a Newton Bhabha PhD Placement Award. S.T.A.I. was supported through the Merit Scholarship Programme for High Technology administered by the Islamic Development Bank. T.H. gratefully acknowledges support from the Deutsche Forschungsgemeinschaft (Cluster of Excellence RESOLV, EXC1069) and the Volkswagen Foundation (LigH2t). F.A.A. is a Royal Society–Wolfson Research Merit Award holder.

- Armstrong FA, Hirst J (2011) Reversibility and efficiency in electrocatalytic energy conversion and lessons from enzymes. *Proc Natl Acad Sci USA* 108:14049–14054.
- Hexter SV, Grey F, Happe T, Climent V, Armstrong FA (2012) Electrocatalytic mechanism of reversible hydrogen cycling by enzymes and distinctions between the major classes of hydrogenases. *Proc Natl Acad Sci USA* 109:11516–11521.
- Hexter SV, Esterle TF, Armstrong FA (2014) A unified model for surface electrocatalysis based on observations with enzymes. *Phys Chem Chem Phys* 16:11822–11833.
- Abou Hamdan A, et al. (2012) Understanding and tuning the catalytic bias of hydrogenase. *J Am Chem Soc* 134:8368–8371.
- Hansen HA, Varley JB, Peterson AA, Nørskov JK (2013) Understanding trends in the electrocatalytic activity of metals and enzymes for  $CO_2$  reduction to  $CO$ . *J Phys Chem Lett* 4:388–392.
- Jones AK, Sillery E, Albracht SPJ, Armstrong FA (2002) Direct comparison of the electrocatalytic oxidation of hydrogen by an enzyme and a platinum catalyst. *Chem Commun (Camb)* 2002:866–867.
- Alonso-Lomillo MA, et al. (2007) Hydrogenase-coated carbon nanotubes for efficient  $H_2$  oxidation. *Nano Lett* 7:1603–1608.
- Hambourger M, et al. (2008) [FeFe]-hydrogenase-catalyzed  $H_2$  production in a photoelectrochemical biofuel cell. *J Am Chem Soc* 130:2015–2022.
- Matsumoto T, et al. (2014) [NiFe]Hydrogenase from *Citrobacter* sp. S-77 surpasses platinum as an electrode for  $H_2$  oxidation reaction. *Angew Chem Int Ed Engl* 53:8895–8898.
- Armstrong FA, et al. (2016) Guiding principles of hydrogenase catalysis instigated and clarified by protein film electrochemistry. *Acc Chem Res* 49:884–892.
- Madden C, et al. (2012) Catalytic turnover of [FeFe]-hydrogenase based on single-molecule imaging. *J Am Chem Soc* 134:1577–1582.
- Rodríguez-Maciá P, Dutta A, Lubitz W, Shaw WJ, Rüdiger O (2015) Direct comparison of the performance of a bio-inspired synthetic nickel catalyst and a [NiFe]-hydrogenase, both covalently attached to electrodes. *Angew Chem Int Ed Engl* 54:12303–12307.
- Priyadarshani N, et al. (2016) Achieving reversible  $H_2/H^+$  interconversion at room temperature with enzyme-inspired molecular complexes: A mechanistic study. *ACS Catal* 6:6037–6049.
- Lubitz W, Ogata H, Rüdiger O, Reijerse E (2014) Hydrogenases. *Chem Rev* 114:4081–4148.
- Berggren G, et al. (2013) Biomimetic assembly and activation of [FeFe]-hydrogenases. *Nature* 499:66–69.
- Knörzer P, et al. (2012) Importance of the protein framework for catalytic activity of [FeFe]-hydrogenases. *J Biol Chem* 287:1489–1499.
- Peters JW, Lanzilotta WN, Lemon BJ, Seefeldt LC (1998) X-ray crystal structure of the Fe-only hydrogenase (CpI) from *Clostridium pasteurianum* to 1.8 angstrom resolution. *Science* 282:1853–1858.
- Adams MWV (1987) The mechanisms of  $H_2$  activation and  $CO$  binding by hydrogenase I and hydrogenase II of *Clostridium pasteurianum*. *J Biol Chem* 262:15054–15061.
- Winkler M, Kuhlert S, Hippler M, Happe T (2009) Characterization of the key step for light-driven hydrogen evolution in green algae. *J Biol Chem* 284:36620–36627.
- Bard AJ, Faulkner LR (2001) *Electrochemical Methods: Fundamentals and Applications* (Wiley, New York).
- Bertoluzzi L, Lopez-Varo P, Jimenez Tejada JA, Bisquert J (2016) Charge transfer processes at the semiconductor/electrolyte interface for solar fuel production: Insight from impedance spectroscopy. *J Mater Chem A Mater Energy Sustain* 4:2873–2879.
- Pandey K, Yadav P, Mukhopadhyay I (2015) Elucidating the effect of copper as a redox additive and dopant on the performance of a PANI based supercapacitor. *Phys Chem Chem Phys* 17:878–887.
- Yadav P, Tripathi B, Pandey K, Kumar M (2014) Recombination kinetics in a silicon solar cell at low concentration: Electro-analytical characterization of space-charge and quasi-neutral regions. *Phys Chem Chem Phys* 16:15469–15476.
- Goldet G, et al. (2009) Electrochemical kinetic investigations of the reactions of [FeFe]-hydrogenases with carbon monoxide and oxygen: Comparing the importance of gas tunnels and active-site electronic/redox effects. *J Am Chem Soc* 131:14979–14989.
- Foster CE, et al. (2012) Inhibition of [FeFe]-hydrogenases by formaldehyde and wider mechanistic implications for biohydrogen activation. *J Am Chem Soc* 134:7553–7557.
- Moganty SS, Baltus RE, Roy D (2009) Electrochemical windows and impedance characteristics of [Bmim][BF<sub>4</sub>]<sup>−</sup> and [Bdmim][BF<sub>4</sub>]<sup>−</sup> ionic liquids at the surfaces of Au, Pt, Ta and glassy carbon electrodes. *Chem Phys Lett* 483:90–94.
- Zheng J, Moganty SS, Goonetilleke PC, Baltus RE, Roy D (2011) A comparative study of the electrochemical characteristics of [Emim][BF<sub>4</sub>]<sup>−</sup> and [Bmim][BF<sub>4</sub>]<sup>−</sup> ionic liquids at the surfaces of carbon nanotube and glassy carbon electrodes. *J Phys Chem C* 115:7527–7537.
- Gray HB, Winkler JR (2010) Electron flow through metalloproteins. *Biochim Biophys Acta-Bioenerg* 1797:1563–1572.
- Page CC, Moser CC, Chen X, Dutton PL (1999) Natural engineering principles of electron tunnelling in biological oxidation-reduction. *Nature* 402:47–52.
- Schlicht S, et al. (2016) An electrochemically functional layer of hydrogenase extract on an electrode of large and tunable specific surface area. *J Mater Chem A Mater Energy Sustain* 4:6487–6494.
- Vidaković-Koch T, Mittal VK, Do TQN, Varničić M, Sundmacher K (2013) Application of electrochemical impedance spectroscopy for studying of enzyme kinetics. *Electrochim Acta* 110:94–104.
- Rumpel S, et al. (2015) Structural insight into the complex of ferredoxin and [FeFe] hydrogenase from *Chlamydomonas reinhardtii*. *ChemBioChem* 16:1663–1669.
- Katz E, Willner I (2003) Probing biomolecular interactions at conductive and semiconductive surfaces by impedance spectroscopy: Routes to impedimetric immunosensors, DNA-sensors, and enzyme biosensors. *Electroanalysis* 15:913–947.
- Adams MWV, Eccleston E, Howard JB (1989) Iron-sulfur clusters of hydrogenase I and hydrogenase II of *Clostridium pasteurianum*. *Proc Natl Acad Sci USA* 86:4932–4936.
- Henstridge MC, Laborda E, Rees NV, Compton RG (2012) Marcus-Hush-Chidsey theory of electron transfer applied to voltammetry: A review. *Electrochim Acta* 84:12–20.
- Léger C, Jones AK, Albracht SPJ, Armstrong FA (2002) Effect of a dispersion of interfacial electron transfer rates on steady state catalytic electron transport in [NiFe]-hydrogenase and other enzymes. *J Phys Chem B* 106:13058–13063.
- Esselborn J, et al. (2013) Spontaneous activation of [FeFe]-hydrogenases by an inorganic [2Fe] active site mimic. *Nat Chem Biol* 9:607–609.